Australian Journal of Crop Science AJCS

AJCS 16(02):233-243 (2022) ISSN:1835-2707
doi: 10.21475/ajcs.22.16.02.3397

Estimating water infiltration rate in oxisols under pasture and agriculture management in the Brazilian Savanna with support of a Drone-RGB onboard sensor

Cleberson Ribeiro de Jesuz[1]*, Manuel Eduardo Ferreira[2]

[1]Federal University of Mato Grosso, Department of Geography, 78060-900, Cuiabá – MT, Brazil
[2]Federal University of Goiás, Institute of Social and Environmental Studies, Image Processing and Geoprocessing Laboratory (LAPIG), 74690-900, Goiânia - Goiás – Brazil

***Corresponding author: clebersonjesuz@ufmt.br**

Abstract

Methods for evaluating physical water data are being increasingly supported by modern and practical tools that have become indispensable for field surveys. Among these tools, unmanned aerial vehicles (UAV) equipped with optical, multispectral, and thermal sensors allow carrying out interventions, monitoring, and strategic data collection with significant cost and time reductions. In this research we used a fixed wing UAV (Swinglet CAM, Sensefly) with RGB camera for creating a precise Digital Terrain Model (DTM) aiming to support an assessment of soil water infiltration in areas under pasture and agricultural management, using the Kostiakov model with concentric rings. Thus, we produced a centimetric-resolution DTM for identifying geomorphological features intrinsically linked to the soil water dynamics and and the accurate insertion of the concentric rings in the slopes. Water velocity and infiltration rates were estimated from descriptive statistics of the data obtained with the Kostiakov model. In this way, the application of the potential equation (Kostiakov) made it possible to mathematically construct the determinants of accumulated infiltration and instantaneous velocity, which can then be replicated and updated at various times, changing only the input data that were logarithmized. The results showed a higher infiltration (54%) in the pasture area, while the unmanned aerial vehicle was considered as an essential tool for obtaining a detailed synoptic representation of the natural and anthropic landscape.

Keywords: Geomorphology, Remote sensing, UAV, Land use, Trenches.
Abbreviations: UAVs_Unmanned Aerial Vehicles; RPAS_Remotely Piloted Aircraft Systems; GSD_Ground Sampling Distance; DTM_Digital Land Model; GNSS Global Navigation Satellite System; PPP_Precision Point Positioning; TR_Trenches; PA_ Control Points; DSM_Digital Land Model.

Introduction

When considering water interactions in natural systems, it is important to identify, delimit, and evaluate the components of the physical environment to understand how they influence water–soil processes either directly or indirectly (Lin et al., 2015).

In the last decade, the parameterization of physical conditioning factors has been made faster and more precise by technologies that have enabled this qualitative-quantitative advancement, especially in terms of collection speed and scale enhancement, as well as in the use of diversified sensors (Watts et al., 2012; Colomina and Molina, 2014).

Unmanned Aerial Vehicles (UAVs), also known as remotely piloted aircraft systems (RPAS), or drones, are being increasingly used because of advances in the accuracy, accessibility, and quality of the iron board sensors for acquiring data (e.g. Lidar and optical sensors) (Maes et al., 2017).

This technology, together with the methods of aerial photogrammetry, remote sensing, and geoprocessing, can be potentially used in surface mapping/geomorphology (Hugenholtz et al., 2013), measuring microtopography and surface runoff (Darboux and Huang 2003), and landslides and mass movements (Niethammer et al., 2012).

The use of UAVs equipped with different types of sensors has made it possible the acquisition of agro-environmental (Dandois et al., 2015; Näsi et al., 2015) and urban (Quin, 2014) data, as well as of world heritage sites (Vetrivel et al., 2015).

However, some standards and models still require in situ measurements using techniques and methods tested and validated in different conditions, as they have specific characteristics in which the evaluation practice is backed up by certain practical procedures (Barros et al., 2014).

Parameters of extreme importance for environmental studies such as the infiltration rate and water velocity in soil, for instance, are usually determined with great effort using in situ methods (Torrado et al., 2005; Da Paixão et al., 2009).

Water entry into the natural system occurs basically by the direct incidence of aqueous material on the surface of the soil which, through infiltration, interacts with the system,

transforming it, altering it, and serving as a solution for other processes (Lorenzon et al., 2015; Cecilio et al., 2013). Thus, water infiltration is of extreme importance to the system as, in many cases, it is directly linked to the water balance in the root zone and surface runoff (Panachuki et al., 2010), which is a precursor of phenomena associated with erosion during rainfall events. Thus, water infiltration is vital for the management of soil and water resources (José et al., 2013).

Modelling the process of water entry into surface and subsurface systems is a fundamental part of the evaluation of water stress damage in plants, aquifer supply rates, and control of high-risk situations in slopes and areas susceptible to erosive processes (Da Costa et al., 1999; Santos et al., 2011).The use of traditional techniques with heavy use of robust equipment, which often require a large workforce, confirms the need to use higher quality/precision spatial data in order to potentiate point insertions of these dense collections, in a faster condition. By making these two approaches viable, a synoptic and precise diagnosis of the area of study can be obtained (Flener et al., 2013; Suomalainen et al., 2014).

There is already a vast literature on aerial photography surveys made with UAVs (or drones). Orthomosaic images and 3D models are powerful tools for small-scale terrain modelling (centimetric or millimetric resolution) (Boon et al., 2016; Cunliffe et al., 2016). High-resolution terrain models, in parallel with interpretations of landscape features, produce materials with greater spatial accuracy and better reliability, as well as the possibility of measuring temporal increments in the data evaluated (Goetz et al., 2018).

The objective this study was to create and analyze terra in topography metrics using high spatial resolution images obtained by UAV, in sites with contrasting land-uses (pasture, agriculture, and remnants of native vegetation) in east center of Mato Grosso, and integrate the suborbital data for the production of materials on a centimetric scale over the physical parameters (topographic features). More specifically, we expected to understand the dynamics of topography and slope orientation, supporting the calculation of water infiltration rates in the soil, and validating the model using descriptive statistics.

Results and Discussion

Products obtained with UAV support

After the post-processing and evaluation of the image data (using the software PIX4D Mapper), aerial photogrammetric mosaics in the visible bands were generated from the data collected with the UAV Swinglet CAM (planned and controlled by E-motion software). The UAV was equipped with an RGB sensor, which facilitated characterizing the slopes in the study area. Another product of post-processing was the 10 cm resolution Digital Land Model (DSM). The DTM shows a hypsometric amplitude of 128 mover an approximately 5 km distance between the highest and lowest points, he was 2.56% topographic gradient (Fig. 1).

The DTM revealed very peculiar phenomenon of the studied area, the formation of a topographic 'neck' (Fig. 2), which directly affects the water and pedological dynamics of the slopes by softening the upper thirds of them, which contributes to the water physical processes (Fig. 3), especially in the lateritic deposits in the imaged area.

Interpretation of the DTM by means of aerial photogrammetry methods allowed identifying the points most suitable within the study area for placing the infiltration rings and digging pedological trenches. The data analyzed from flight information with the UAV enabled the interpretation of the best sample points within the studied cut out, for allocation of the infiltration rings and the opening of the pedological trenches and the lines of control points across the two types of land-use, mechanized agriculture and extensive livestock ranching, in order to supplement the physical-hydric information of this area and support the discussion.

Hydrophysical condition of the slopes

This analysis aimed to understand how the soil hydrophysical characteristics correlate with the slopes under livestock ranching or agriculture, especially in relation to water infiltration, and how its dispersion is modified in the sense that it moves between the top and base of the slopes (Fig. 4).

The granulometric data collected from the trenches and control points showed a high proportion of sand in the samples. Coarse sand is more abundant in the upper and lower thirds of the slopes under livestock ranching, where they represent an average of 2% and 6.4% at the top and base of the slope, denoting that the movement and surface and subsurface removal of material act strongly on the flow dynamics.

The reductions in granulometric values according to the movement of the upper and lower thirds are correlated with the increase in silt at the base of the slopes, especially in trenches TR3 and TR6 (Fig. 4), and with lower values in the control points (Table S1). These results show a greater structuration of the original soils in the lower third; there is a notable relationship between the distribution of fine sand and silt, presenting inversely proportional rates along the slope profile, validating the structure of the Yellow Latosol, which presents a consistently low clay content and high percentages of silt and sand, 22% and 75%, respectively.

The refined dynamics in the trench collections, due to the stratification analysis of each horizon, exposes a more particular feature between slopes with contrasting land use. The sand percentage in slopes under mechanized agriculture is, on average, 21% higher than in slopes under pasture, reflecting an inverse relation with the clay contents, as this was 35% and 19% on average, in trenches in pasture and agriculture slopes, respectively.

The relationship between the sand and clay contents and land use is better evidenced in the lower third of the slopes, especially in TR3 (livestock) and TR6 (agriculture). In TR3, it is possible to notice an increase with depth in the profile, reaching a maximum of over 45%. In TR6, the medium and fine sand fractions are over 50%, with a considerable decrease in the clay fraction.

Another contrast between the two slopes, when analyzing the control points, is the clay fraction, which is over 50% higher in the livestock slope than in agriculture slopes, denoting a more intense physic chemical activity in the soil, derived from local pedogenetic conditions. This greater activity conditioned clear differentiations in particle size and in their distribution on the points sampled, that is, in the soil texture.

Table 1: Linearized equations of the Kostiakov method for cumulative infiltration data.

Location of the concentric ring	Equations ($I = K.T^a$)
Livestock 1 (top)	$I=0.028244112 * T^{-70424504507531}$
Livestock 2 (middle third)	$I=0.097771612* T^{1.22546016294832}$
Livestock 3 (lower third)	$I=0.357640109* T^{1.02362533650328}$
Agriculture 1 (top)	$I=0.736473754* T^{0.953716170209483}$
Agriculture 2 (middle third)	$I=0.774727966* T^{1.02038178761977}$
Agriculture 3 (lower third)	$I=1.529838755* T^{1.16558751544592}$

Source: Field data collected.

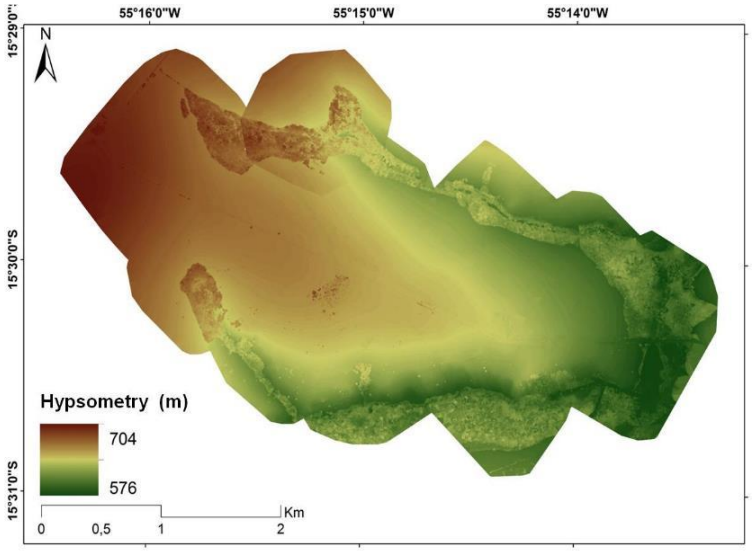

Figure 1. The 10 cm resolution digital surface model.

Table 2. Main variables of linear regressions for infiltration rings.

Sampling	R	R^2	a	b	F-Sig	P-value	LL	UL
Livestock 1	0.960	0.922	-1.54907	1.704245	1.46439E-12	-1.08E-07	-1.9509961	-1.147148065
Livestock 2	0.944	0.891	-1.00979	1.22546	1.22316E-08	0.0011191	-1.5455411	-0.0474033352
Livestock 3	0.998	0.997	-0.44655	1.023625	4.57653E-48	1.143E-23	-0.4834275	-0.4096800
Agriculture1	0.999	0.999	-0.13284	0.953716	3.73073E-38	2.657E-12	-0.1534651	0.112220302
Agriculture 2	0.999	0.998	-0.11085	1.02038	3.21374E-36	2.461E-08	-0.13905514	-0.082650102
Agriculture 3	0.996	0.992	0.18464	1.16558	4.1793E-26	9.264E-07	0.12699441	0.24229691

Legend: R: R-Multiple; **R^2**: R-Square; **a**: Intercept; **b**: Log (I); **F-Sig**: Significance of Regression, **P-value**: Significance level, **LL**: Lower limit; and **UL**: Upper limit. **Source**: Regression of field data.

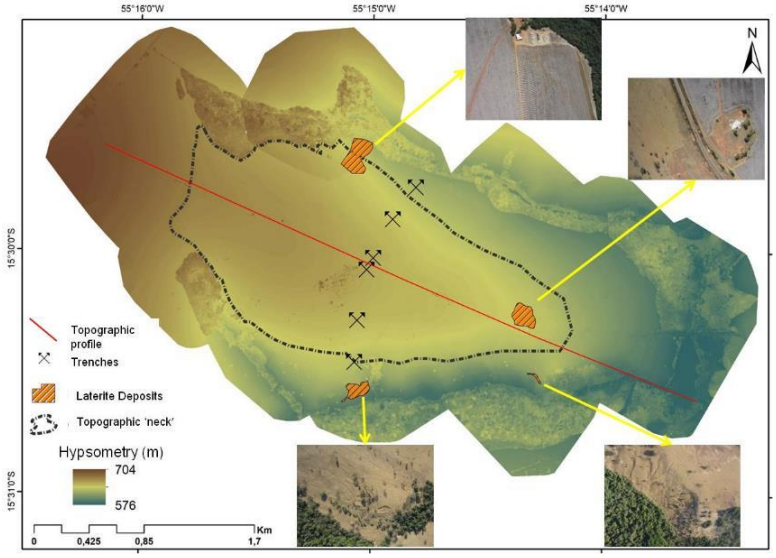

Figure 2. Digital land model of the study area, with emphasis on the pedo-geomorphological formation of the topographic 'neck'.

Table 3. Land use in the study area, Campo Verde, Mato Grosso.

Identification/Use	Period	Crops and General Management
Extensive livestock production	1970/1975	Native vegetation removal.
	1975/2016	Bread grass (Brachiaria brizantha) pasture, 1.5 t ha^{-1} of dolomitic lime every 3 years.
Agriculture: soy/maize/cotton	1970/1975	Native vegetation removal.
	1975/1990	Bread grass pasture, 1.5 t ha^{-1} of dolomitic lime every 3 years.
	1990/1992	Pasture removal followed by conventional soybean plantation.
	1992/2004	Bread grass pasture replantation, 1.5 t ha^{-1} of dolomitic lime every 3 years.
	2004/2009	Pasture removal, followed by soybean plantation, and rotation with out-of-season maize in the conventional system.
	2009/2016	Implementation of out-of-season cotton in the soybean/maize system.

Source: Field interviews conducted.

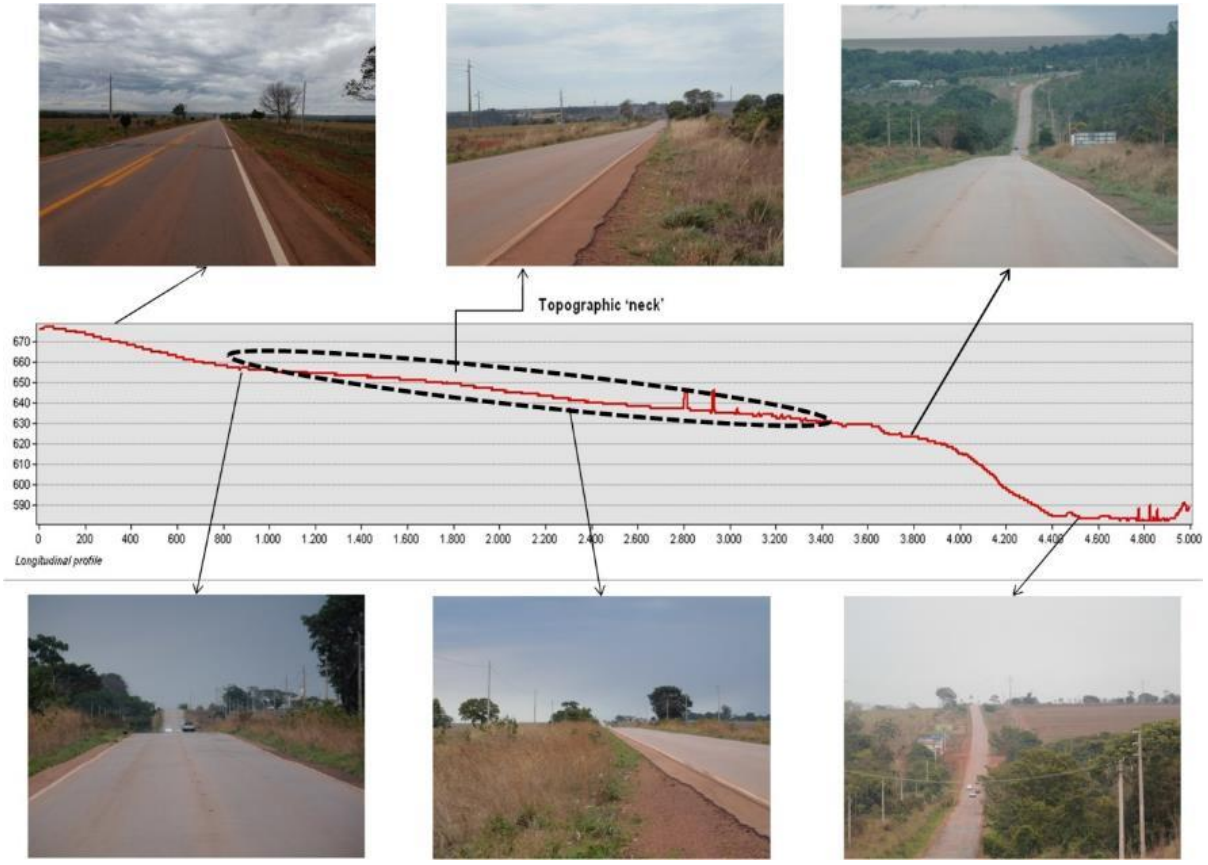

Figure 3. Longitudinal profile, highlighting the topographic 'neck' area, evidenced by highway MT 140.
Source: Field data collected by the authors.

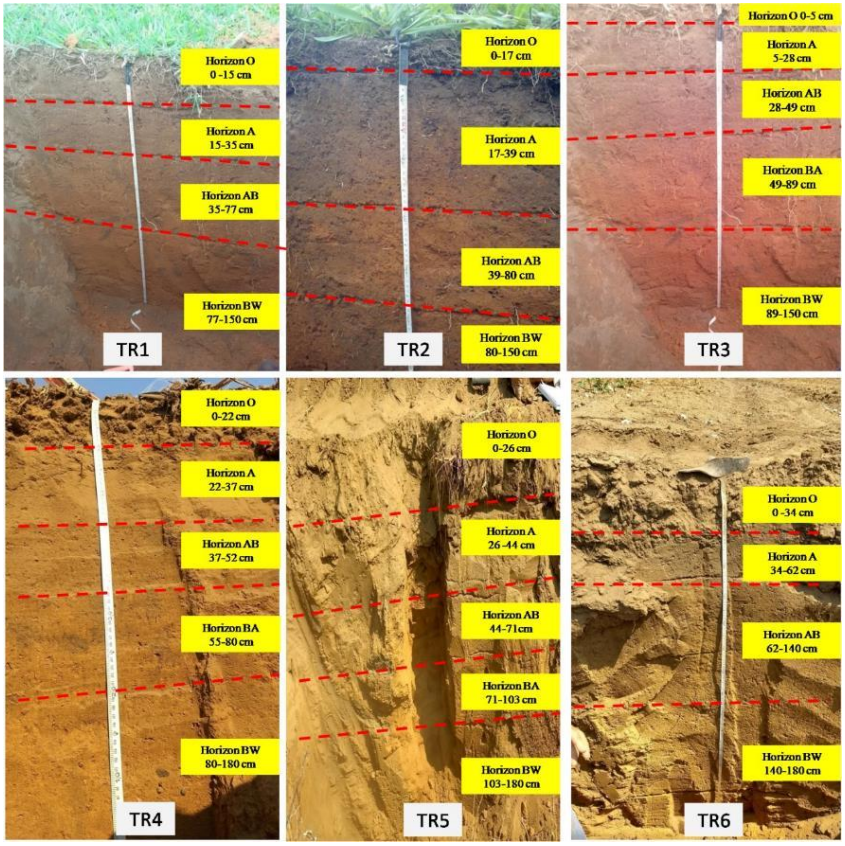

Figure 4. Trenches: pasture (TR1, TR2, and TR3) and agriculture (TR4, TR5, and TR6).

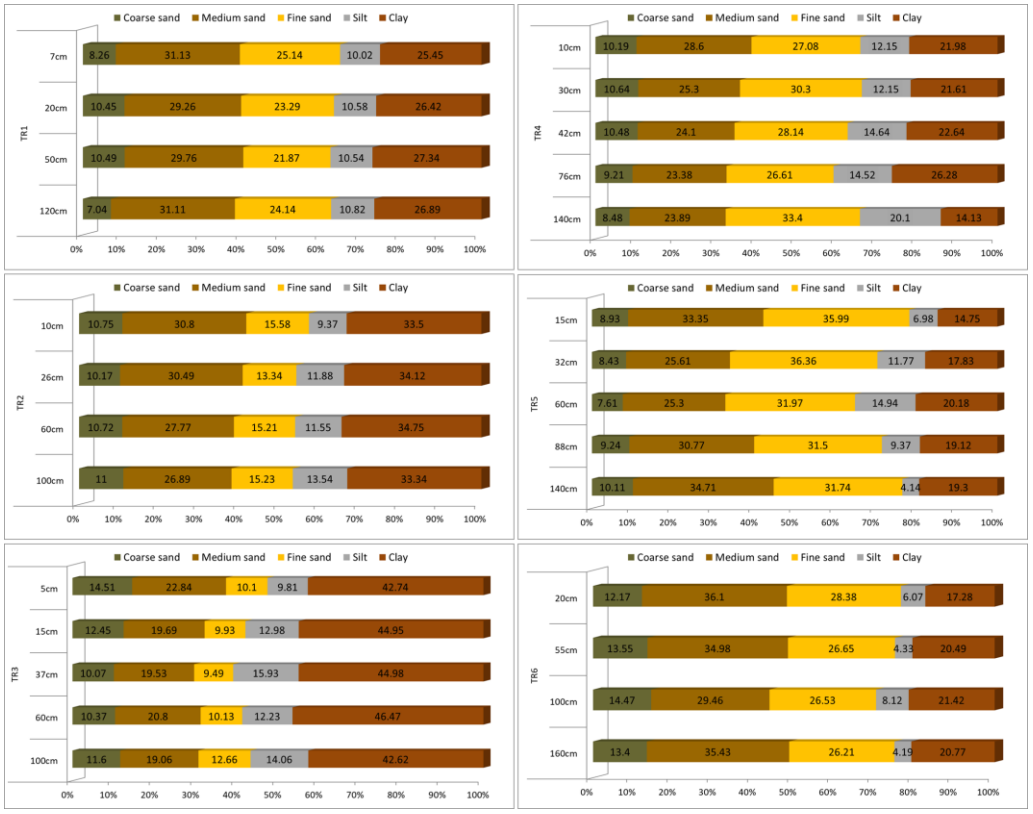

Figure 5. Distribution of granulometry in the samples analyzed, as a function of depth in the pedological trenches.
Source: Field data collected by the authors.

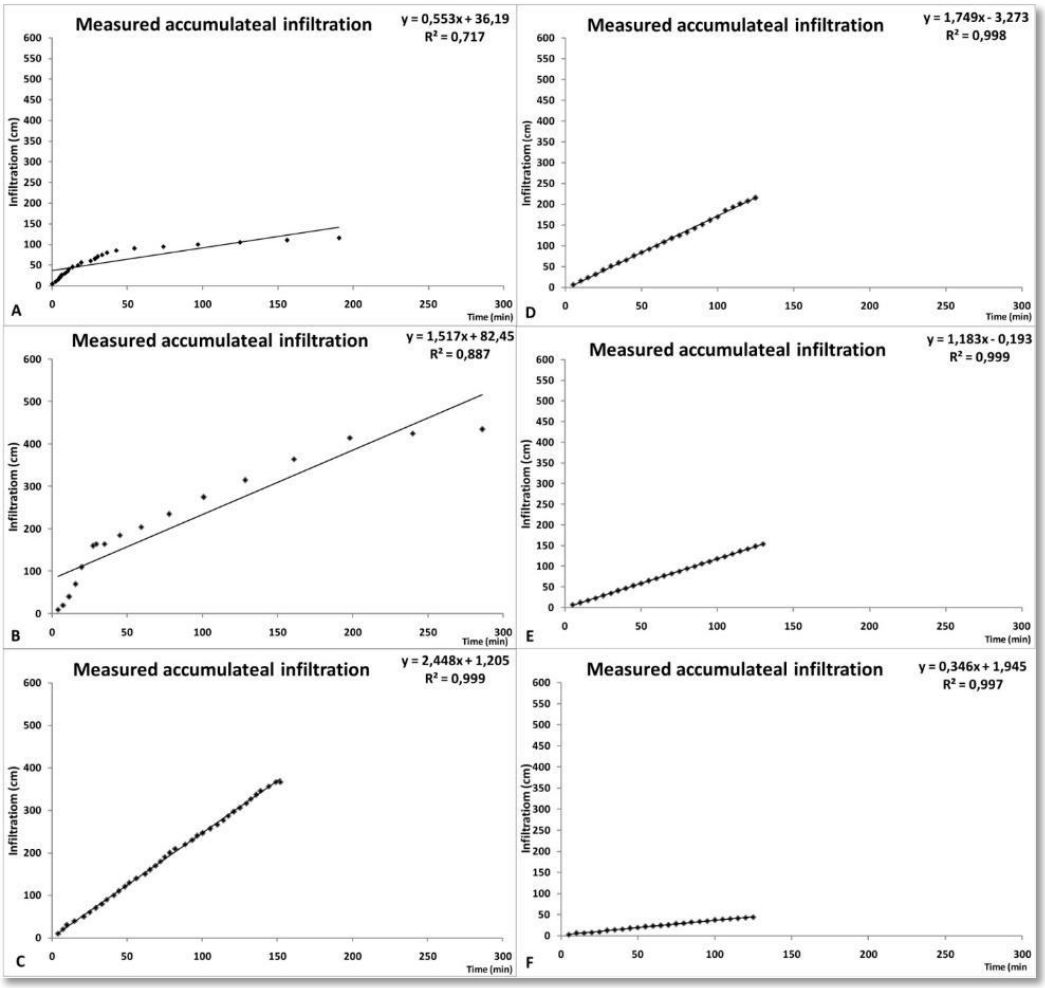

Figure 6. Infiltration graphs for the concentric rings. A, B, and C show water infiltration in pasture areas. D, E, and F correspond to mechanized agriculture areas.
Source: Field data collected by the authors.

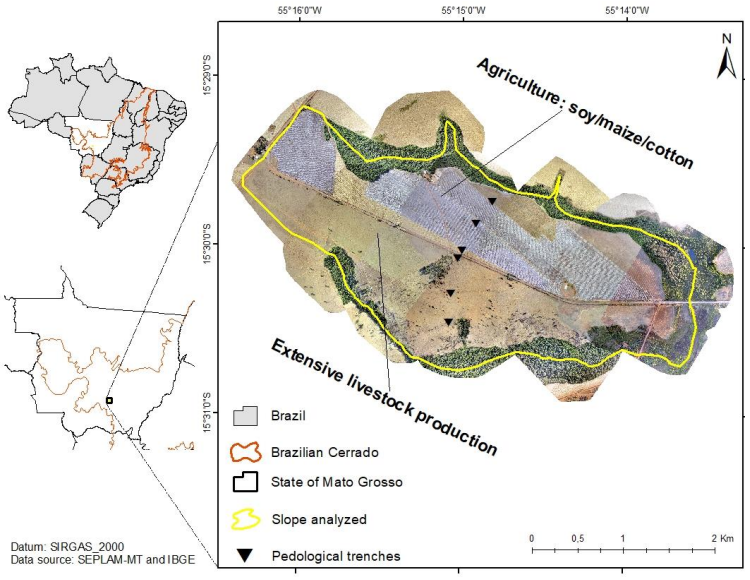

Figure 7. Study area illustrated with aerial image obtained by an UAV on August 2016, showing the sampling points with rings and pedological trenches.

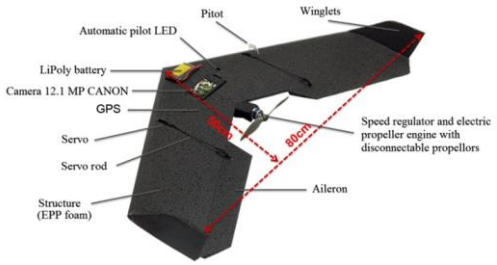

Figure 8. Top view of the UAV Swinglet CAM, Sensefly, and Canon IXUS 220 HS camera.

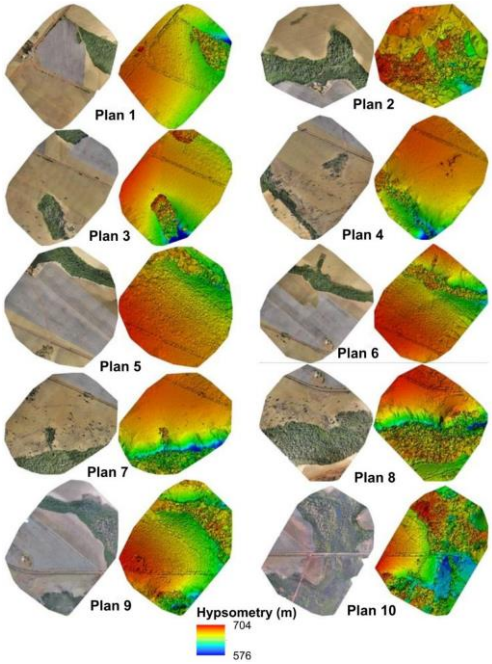

Figure 9. RGB mosaic of the 10 flight plans, with the resultant Digital Land Model.

Figure 10. Installation of concentric infiltration rings for monitoring soil infiltration in areas of (A and B) pasture and (C and D) agriculture.
Source: Field data collected by the authors.

Figure 11. Digging trenches in areas of (A and B) pasture and (C and D) agriculture. **Source:** Field data collected.

Trench assessments and the vertical distribution of the horizons were fundamental for understanding the relationships between the soil hydrophysical components, indicating the points most suitable for installing the infiltrators. Therefore, the findings subsidized the most suitable points of contribution and precision for soil moisture analysis. Data based on the infiltration variable, determined using the concentric ring method, and were used to evaluate the declivity-infiltration relationship. First, the exponential data were linearized to fit the potential equation method or Kostiakov model (Fig. 6).

Charts **A** and **B** in Fig. 6 show a pronounced increase in humidity during the first 50 minutes. These infiltration rings were installed at the top and middle thirds of the slope. This means low soil moisture at the surface and subsurface horizons. However, chart **C**, which is in the lower third of the slope, shows a progressive, more homogeneous an increasing trend.

In the same data set, the infiltration values at centimetric depths are also diverse, especially in charts **B** and **C**, which presented more than 450 cm and 350 cm, respectively, while chart **A** presented only 120 cm. The outline of these charts is graph **B**, which, because it is in the middle third in the area of completion of the topographic 'neck', has a simultaneous time superior to the charts **A** and **C**, in 42.8% and 54.2%, respectively, which may indicate a direct action of the laterite deposit, acting horizontally on the profile.

This same data set shows a good correlation between infiltration and the elapsed time, as the lines with the respective R^2 values indicate percentages higher than 60% (Silva et al., 2017). However, charts **A** and **B** show intercept (predicted value at zero minutes) values between 36.19 cm and 82.45 cm.

Charts **D**, **E**, and **F** represent the infiltration rings installed in slopes under mechanized agriculture and show similar growth lines at the times of infiltration. Chart **E** shows the lowest infiltration depth, 79.1% and 75% lower than those of charts **D** and **F**, with both plotted concomitantly at the top and middle thirds of the slope. Another factor that explains this circumstance is its location in the lower third of the slope, where there is a greater presence of hydromorphic soils.

The values of the direct correlation between the infiltration and elapsed time are at levels of high ratio, on average 93%, with intercepts of a maximum of 3.2 cm for predicted values.

The exponential (i.e., experimental) infiltration data, when processed by the Kostiakov equation ($\mathrm{I} = \mathrm{K}.\mathrm{T}^{\mathrm{a}}$), became part of a linearization; that is, a line where$\mathrm{Y} = \mathrm{b} * \mathrm{X} + \mathrm{a}$, when logarithms are applied to both sides of the equation and analyzed via linear regression. Thus, the linearized data of cumulative infiltration are regulated by the equations shown in Table 1.

In order to present the main patterns of infiltration in this terrain, the linear regression data, based on the linearized data, are shown in Table 2.

The values of linear regression based on the linearized data show high correlation values, as a result of the data set analyzed, with an average 0.983 (R-Multiple).

In this sense, the values of higher differentiation are those of Livestock 2, of the middle third of the slope, where the R-Multiple was 94%; only 6% of the total data cannot be accounted for by this equation. The R-Squared denotes an 11% of non-correlation between the analyzed pairs of variables. This can be explained by three large residuals of observations 1 (0.281), 16 (0.168), and 17 (0.233).

Livestock 1 also shows values of R-Multiple and R-Squared lower than the average (96% and 92%); as well as their F (237) statistics, these factors are linked to points in the data set, with values above the general framework, distorting its explanatory relationships, and logarithmic pairs of variables. However, the level of significance is generally high.

The other samplings of the regressions are presented with values of explanation by the proposed equation, and correlation of the pairs of variables used with high

correspondence rate. Its values of level of significance and limits, both lower and higher, are in the normality of the general framework of the analyzed samplings.

In the present data, the relationship between the infiltration rate and percolation of the centimetric depth water, in slopes containing Yellow Latosol and low amplitude clinography, shows that water is one of the main factors of pedogenic alteration. Thus, the action of water has been fundamental for the spatiotemporal evolution of the morphological configuration of the Planalto dos Guimarães region, or others with similar physical and biotic situations.

Material and Methods

Study area

The study encompassed two areas with contrasting land use, pasture and mechanized agriculture, both located in the municipality of Campo Verde, eastern Mato Grosso, Brazil between 15°28'30" and 15°31'44"South and 55°16'12" and 55°13'33"West, encompassing an area of 7.86 km² (Fig. 7).

According to Moreira and Borghi (1999), the geological formations present in the study area are Ponta Grossa, and contacts with Furnas. The Ponta Grossa formation is lithologically defined by siltstones and fine sandstones; brachiopod fossils are common in siltstone. The Furnas formation presents the base for the top is represented by conglomerate sandstones that scale to pure white to yellowish sandstones, locally purplish, with hummocky cross stratifications that in turn pass sandstones with stratifications crossed by waves.

The relief units found are linked to the morphostructure of the Paraná Sedimentary Basin, more precisely its northern border, with Chapada and Planalto dos Guimarães as its morphological and sculptural unit (Ross, 2014). Morphoescultural unit of flat relief, with elevations ranging from 600 to 800m, which presents processes of dissection of the terrain, with tabular tops, and low drainage density.

Soils are predominantly Yellow Dystrophic Oxisols, with Gleisols/Floss Neossols in the lower thirds of the slopes (area in contact with water courses), making it possible the appearance of Dystrophic Plinthosols in these areas, with strong action of water in its pedogenetic structure.

The climate prevailing in the area where the study slopes are located is classified as alternating between a continental tropical and wet or dry climate in the plateaus and depressions of Mato Grosso, respectively, with an average rainfall between 1880–2100 mm/year, with the period from October to May as the rainy season (Tarifa, 2011).

One of the predominant features of the land use and land cover in the study area is the suppression of native vegetation (Cerrado biome) as a result of the occupation and transformation to agro pastoral activities that has been ongoing since the 1970s (Table 3).

UAV Photogrammetric Survey

The procedures for using the UAV Swinglet CAM (Fig. 8) consisted primarily of developing the flight plans using the software E-motion (electronic monitoring station), including the determination of the longitudinal and lateral coverage of the photos, and the ground pixel size, known as the ground sampling distance (GSD), which in this case was 0.10 m. The point cloud from the Digital Land Model (DTM) also follows this GSD. The use of UAV meets many of the criteria listed by James et al., (2019) in the use of photogrammetry techniques.

The sensor used was a standard RGB digital camera, Canon IXUS 220 HS, with 12.1 megapixels of spatial resolution, equipped with a 1/2.3" (4000 × 3000 pixel) CMOS sensor, pixel pitch of 1.54 μm, and equivalent focal length of 35 mm CAM.

For the present study, 10 flights were performed each one covering an area of 1.2 km². A total of 633 photographs were collected during the flights, at an elevation of 331 m, with 60% and 40% of longitudinal and latitudinal overlap, respectively (Fig. S1).

To carry out the flights, it was necessary to create control points on the ground, distributed so to encompass all the areas covered by the flight plans. Each point was marked on the soil by a white painted circle, following the methodology of Wolf (2004), and was located with a Global Navigation Satellite System (GNSS), which provided an area three times larger than the proposed GSD. The geodetic surveys were carried out with a pair of Topcon Hiper Plus II GNSS receivers, and the base coordinates were determined by precision point positioning (PPP), using a continuous monitoring station at the Brazilian Institute of Geography and Statistics (IBGE, http://www.ppp.ibge.gov.br/ppp.htm), with a 0.001 gms latitude error, 0.002 gms longitude error, 0.005m elevation error, and 1.09 m geoid undulation. The PPP method allows installing the GNSS base in remote locations, without a geodesic frame or known coordinates, using post-processing to the base and points sampled with corrections by the rover.

The flights were carried out in August 2016 (dry season), after the harvest periods of soybean, maize, and cotton, between 11:00 h and 15:00 h. In this period of the year, the vegetation was in a less vigorous state, which facilitated locating the ground control points and make the DTM adjustments (Fig. S2).

The photographs acquired during the flights were subjected to digital and technical mosaic/orthorectification processing using the PIX4D Mapper software (Fig. 9) (Albuquerque et al., 2020), following the methods described by Alves Jr. et al., (2018). This yielded the final product, a 10cm spatial resolution digital land model (DTM).

Field procedures

Based on the georeferenced, centimetric resolution land cover and relief modelling information (i.e., orthomosaic and DTM), the sites most suitable for placing points for measuring soil infiltration were located. Infiltration rings were installed on the upper, medium, and low parts of the slopes (Fig. 10).

After choosing the point, taking into account the position on the vertical topography (i.e., upper, medium, or low strand position) for installing the rings, pedological trenches were dug to examine the soil horizon structure and how the water behaves at the chosen points (Fig. 11). For achieving soil granulometry data in the horizons of the trenches, at depths of 0–20 cm, 20–40 cm, and 40–60 cm, the control points were used following an average distance of 100m between them, interspersed between trenches, so that there are two points of distance between them.

An identification code was assigned to each point: trenches and control points in the livestock area were coded as TR1 to

TR3 and P100 to P600, respectively; those on agricultural land were coded as TR4 to TR6 and PA100 to PA400, respectively. The different number of control points was due to the impossibility of collecting materials close to the watercourse in the mechanized agriculture area, due to the agronomic treatment that was being applied by the farm owners.

The UAV data and in situ standard assessments enabled determining specific features of the slopes, elucidating water behavior in the superficial and clinographic systems of the study area.

Statistical analysis

The statistical analyses for calculating accumulated infiltration from the concentric infiltration rings (non-parameterized) data, were carried out using the potential equation or Kostiakov model (Eq.1), as shown by Santos et al. (2016).

$I = K.T^a$ (Eq. 1)

Where:

I = Accumulated infiltration (cm);

K = A parameter dependent on the initial moisture of the soil;

T = Infiltration time (min);

a = Soil-dependent constant, varying between 0 and 1.

The input data for this equation are exponential; however, the coefficients a and K need to be in analytical mode to be determined. Thus, by taking logarithms of both sides of Eq.1, a linear regression method can be used (Eq. 2):

$\log I = \log K + a.\log T$(Eq. 2).

This is a simple linear equation of the form I=A+B.X (Eq. 3), where:

Y = logI;

A = logK;

B = a

X = logT.

Thus, the values of A and B are estimated using the following expressions (Eq. 4 and 5):

$A = \frac{\sum X \times \sum XY - \sum X^2 \times \sum y}{(\sum X)^2 - m \times \sum X^2}$ (Eq. 4);

$B = \frac{\sum X \times \sum Y - m \times \sum XY}{(\sum X)^2 - m \times \sum X^2}$ (Eq. 5),

where, m is the number of data pairs I, T.

A = log K, K = antilogA, thus, $K = 10^A$

B = a, thus, a = B.

Thus, once the values of A and B have been estimated, the parameters K and a of the original exponential equation can be obtained as K is the antilog of A, and a equals B.

Conclusions

The use of the UAV in constructing digital elevation models at a detailed scale was fundamental for understanding the morpho-pedological dynamics of the study slopes, as well as to check the topographic 'neck' and laterite deposits, structural determinants of the local geomorphology, and thus the soil type found in the area. The RGB data acquired with the optical digital camera coupled to the UAV, associated with field surveys of granulometry (i.e., exploratory and descriptive analyses in trenches), constitute a suitable method for evaluating water infiltration with the Kostiakov model. All the six points examined showed a good correlation.

Regarding land use, the most noticeable feature between the contrasting slopes was that the percentage of sand in mechanized agriculture was, on average, 21% higher than in pasture. This reflects an inverse relationship when the clay distribution is observed, where in the trenches of the slope with pasture, the average clay percentage is 35%; the agriculture slopes presented a percentage of 19%, which is higher than in the livestock area, which presented values of around 15% (Fig. S3).

The information on the physical components of the soil and the specificities of the systematized use and occupation, added to the specific conditions of the study slopes, are fundamental for understanding the soil moisture dynamics and potential impacts for the studied areas.

The use of geotechnologies, associating field data with high-resolution imagery/map, generates products with high cartographic quality, and should be encouraged, taking into account the capacity of available equipment, as well as access to representative realities.

Acknowledgments

This work was supported by the first author's doctoral scholarship, proposal: GM/GD-Cotas of the Graduate Program, Process Number: 141813/2015-6 of the National Council for Scientific and Technological Development - CNPq/Brazil. M.E.F. is CNPq Research Fellow (grant #315699/2020-5).

The authors thank the National Council for Scientific and Technological Development - CNPq/Brazil, which granted a scholarship to the first author (#141813/2015-6). We are also grateful to the Graduate Program in Environmental Sciences (CIAMB) at the Federal University of Goiás, Brazil, which financed this publication. M.E.F. is a CNPq Research Fellow (grant #315699/2020-5).

References

Albuquerque RW, Costa MO, Ferreira ME, Carrero GC, Grohmann CH (2020) Remotely piloted aircraft imagery for automatic tree counting in forest restoration areas: a case study in the Amazon. J Unma Veh Syst. 8: 207-223

Alves Jr LR, Ferreira ME, Cortes JBR, Jorge LAC (2018) High accuracy mapping with cartographic assessment for a fixed-wing remotely piloted aircraft system. J Appli Rem Sens. 12: 1-22.

Barros CAP, Minella JPG, Tassi R, Dalbianco L, Ottonelli AS (2014) Estimativa da infiltração de água no solo na escala de bacia hidrográfica. R Brasi Ciên do Solo. 38 (2): 557-564.

Boon MA, Greenfield R, Tesfamichael, S (2016) Unmanned Aerial Vehicle (UAV) Photogrammetry Produces Accurate High-resolution Orthophotos, Point Clouds and Surface Models for Mapping Wetlands. S Afric Jour Geom. 5: 186–200.

Cecilio RA, Martinez MA, Pruski FF, Silva DD (2013) Modelo para estimativa da infiltração de água e perfil de umidade do solo. R Brasi Ciên do Solo. 37: 411-421.

Colomina I, Molina P (2014) Unmanned aerial systems for photogrammetry and remote sensing: A review. ISPRS J. Photogramm. R Sens. 92: 79–97.

Cunliffe AM, Brazier R.E, Anderson K (2016) Ultra-fine grain landscape-scalequantification of dryland vegetation structure with drone-acquired structure-from-motion photogrammetry. R Sens Envir. 183: 129–143.

Da Costa ÉL, Da Silva AM, Colombo A, De Abreu AR (1999) Infiltração de água em solo, determinada por simulador de chuvas e pelo método dos anéis. R Brasi Eng Agríc e Ambi. 3: 131-134.

Da Paixão FJR, Andrade ARS, De Azevedo CAV, Costa TL, Guerra HOC (2009) Ajuste da curva de infiltração por meio de diferentes modelos empíricos. P Aplica Agrot. 2: 107-112.

Dandois JP, Olano M, Ellis EC (2015). Optimal Altitude, Overlap, and Weather Conditions for Computer Vision UAV Estimates of Forest Structure. R Sensi. 7: 13895-13920.

Darboux F, Huang C (2003) An Instantaneous-Profile Laser Scanner to Measure Soil Surface Microtopography. Soil Sci. Soc. Sou. J. 67: 92-99.

Flener C, Vaaja M, Jaakkola A, Krooks A, Kaartinen H, Kukko A, Kasvi E, Hyyppä H, Hyyppä J, Alho P (2013) Seamless Mapping of River Channels at High Resolution Using Mobile LiDAR and UAV-Photography. R Sens. 5: 6382-6407.

Goetz J, Brenning A, Marcer M, Bodin X (2018) Modeling the precision ofstructure-from-motion multi-view stereo digital elevation models from repeated close-range aerial surveys. R Sens Envi. 210: 208-216.

Hugenholtz CH, Whitehead K, Brown OW, Barchyn TE, Moorman BJ, Leclair A, Riddell K, Hamilton T (2013) Geomorphological mapping with asmall unmanned aircraft system (sUAS): feature detection and accuracy assessment of a photogrammetrically-derived digital terrain model. Geo. 194: 16–24.

James MR, Chandler JH, Eltner A, Fraser C, Miller PE, Mills JP, Noble T, Robson S, Lane SN (2019) Guidelines on the use of structure from motion photogrammetry in geomorphic research. E Surf Proc Land. 44 (10): 2081-2084.

José JV, Rezende R, Marques PAA, Freitas PSL, De Alves DS (2013) Determinação da velocidade de infiltração básica de água em dois solos do noroeste do estado do Paraná. R Agron e M Ambi. 6: 155-170.

Lin H, Patrick D, Grenn TR (2015) Hydropedology: the last decade and the next decade. Soi Scie Soci Ame. 79: 357–361.

Lorenzon AS, Dias HCT, Tonello KC (2015) Escoamento superficial da água da chuva em um fragmento Florestal de Mata Atlântica, Viçosa-MG. R Bras Agro Sust. 5 (1): 50-58.

Maes WH, Huete AR, Steppe K (2017) Optimizing the Processing of UAV-BasedThermal Imagery. R Sens. 9 (476): 1-17.

Moreira MIC, Borghi L (1999) Fácies sedimentares e sistemas deposicionais das formações Alto Garças e Vila Maria na região de Chapada dos Guimarães (MT), borda noroeste da bacia do Paraná. R Bras Geoc. 29 (3): 419-428.

Näsi R, Honkavaara E, Lyytikäinen-Saarenmaa P, Blomqvist M, Litkey P, Hakala T, Viljanen N, Kantola T, Tanhuanpää T, Holopainen M (2015) Using UAV-Based Photogrammetry and Hyperspectral Imaging for Mapping Bark Beetle Damage at Tree-Level. R Sens. 7: 15467-15493.

Niethammer U, James MR, Rothmund S, Travelletti J, Joswig M (2012) UAV-based remote sensing of the Super-Sauze landslide: Evaluation and results. E Geol. 128: 2–11.

Panachuki E, Bertol I, Alves Sobrinho T, Vitorino ACT, Souza CMA, Urchei MA (2010) Rugosidade da superfície do solo sob diferentes sistemas de manejo e influenciada por chuva artificial. R Bras Ciên do Solo. 34: 443-451.

Quin R (2014) An Object-Based Hierarchical Method for Change Detection Using Unmanned Aerial Vehicle Images. R Sens. 6: 7911-7932.

Ross JLS (2014) Chapada dos Guimarães: Borda da Bacia do Paraná. R Depar Geog (USP). 28: 180-197.

Santos TEM, Montenegro AAA, Silva DD (2011) Umidade do solo no semiárido pernambucano usando-se reflectometria no domínio do tempo (TDR). R Bras Enge Agrí e Ambi. 15: 670–679.

Santos TEM, Souza ER, Montenegro AAA (2016) Modeling of soil water infiltration with rainfall simulator in different agricultural systems. Revista R Bras Enge Agrí Ambi. 20: 513-518.

Silva SHG, Teixeira AFS, Menezes MD, Guilherme LRG, Moreira FMS, Curi N (2017) Multiple linear regression and random forest to predict and map soil properties using data from portable X-ray fluorescence spectrometer (pXRF). Cien Agrot. 41(6): 648-664.

Suomalainen J, Anders N, Iqbal S, Roerink G, Franke J, Wenting P, Hünniger D, Bartholomeus H, Becker R, Kooistra L (2014) Light weight Hyperspectral Mapping System and Photogrammetric Processing Chain for Unmanned Aerial Vehicles**.** R Sens. 6: 11013-11030.

Tarifa JR (2011) Mato Grosso: clima: análise e representação cartográfica. Cuiabá, MT: Entrelinhas. 102p.

Torrado PV, Lepsch IF, Castro SS (2005) Conceitos e aplicações das relações pedologia-geomorfologia em regiões tropicais úmidas. T Ciên do Solo. 2: 4145-4192.

Vetrivel A, Gerke M, Kerle N, Vosselman G (2015) Identification of damage in buildings based on gaps in 3D point clouds from very high resolution oblique airborne images. ISPRS J of Photr and Rem Sens. 105: 61–78.

Watts AC, Ambrosia VG, Hinkley EA (2012) Unmanned Aircraft Systems in Remote Sensing and Scientific Research: Classification and Considerations of Use. R Sens. 4: 1671-1692.

Wolf D (2004) Elements of Photogrammetry with Applications in GIS. 3rd ed. The McGraw-Hill Companies, Boston, Massachusetts.